

0017-9310(94)00353-X

Numerical investigations on thermal effects of laser-ocular media interaction

E. H. AMARA

Centre de Développement des Technologies Avancées, Laboratoire des Lasers et Applications,
128 chemin Mohamed Gacem B.P. 245, El Madania-Alger, Algeria

(Received 2 March 1993 and in final form 4 November 1994)

Abstract—A thermal model of the human eye exposed to laser irradiation is presented. It allows us to compute the intraocular temperature distribution. The physical system is described by a set of partial differential equations consisting of the heat equation that includes the laser heat source, and the boundary and initial conditions equations. The analytical system is transformed to an integral formulation where a Galerkin function is applied. The integral formulation is then treated by the finite elements method to lead to a discrete algebraic system which is solved by numerical methods. We studied the effects of the laser power, the laser wavelength and other parameters. Among the results obtained, it appears that the more the laser wavelength decreases the more the effects on the eye are hazardous, since this is related to the production of a higher temperature that can lead to the denaturation of the ocular tissues.

1. INTRODUCTION

The eye is the organ the most vulnerable to damage by laser radiation. The incident energy is focused on a small area, called the fovea, on the retina, with a resulting increase in the irradiance. High values of the irradiance at the retina can occur even with laser beams which would cause no problem if absorbed by skin. The eye is also the organ which has been most studied in interaction with laser light. With the widespread use of lasers, the eye can be injured during the adjustment or alignment operations. Just after injury, there are different degrees of retinal coagulation, edema or hemorrhage in exposed spots and thus an immediate reduction of visual acuity occurs. The particular combination of exposure parameters such as wavelength, pulsewidth and total energy delivered may result in pathology to either cornea, lens or retina.

Many authors have studied the damage caused to the eye by heat sources. An interesting work [1] has been performed on laser hazardous effects and on human eyes that have been accidentally exposed to laser beams. *In vivo* experiments on the animal eye and theoretical investigations have been achieved. Kramar *et al.* [2] and Emery *et al.* [3] have studied cataract formation on rabbits and monkey eyes under microwave irradiation. Birngruber *et al.* [4] have used a theoretical model to determine the thermal threshold damage on the retina and the results were compared to the experiment. The model predicts a maximum temperature increases between 35 and 65°C in the retina for threshold exposures between 0.3 and 0.001 s. The range of threshold temperatures implies that thermal denaturation of proteins is the cause of the observed damage. Scott [5, 6] has developed a

finite element model of heat transport in human eye to study the cataract formation due to infrared (i.r.) radiation exposure. Lagendijk [7] has used a finite difference method to calculate the temperature distribution in human and rabbit eyes during hyperthermic treatment.

An appropriate way to quantify the laser thermal effects on the eye is to calculate the intra-ocular temperature distribution. In this paper we present a computation work using the finite element method to predict the thermal effects on the eye tissues exposed to laser beam irradiation. Since direct experimentation on the human eye is impossible, numerical simulation is worth doing, even if the physical parameters of the eye are not known with a great precision, and the eye is simulated approximately neglecting some vital features such as nerves, blood vessels, etc. The numerical investigation gives at least a clear view of the effects induced by laser radiation. The laser beam being transmitted by the lens of the eye is focused on the retina, which is the light sensitive medium containing the opaque pigmented layer called the pigment epithelium, the main emphasis in effects of lasers on the eye has been on interactions with the retina, and thus the retinal image that is of interest to us is that which is projected on the fovea, which has a special function and neurology. The fovea being very difficult to model, and although it is anatomically different from retina, we consider in our study that it constitutes a part of the retina and thus has the same thermal properties. Among the statements we make also in our study, it is supposed that the laser energy is focused on the fovea, whereas in reality the radiant energy entering the eye may end up on any part of the retina.

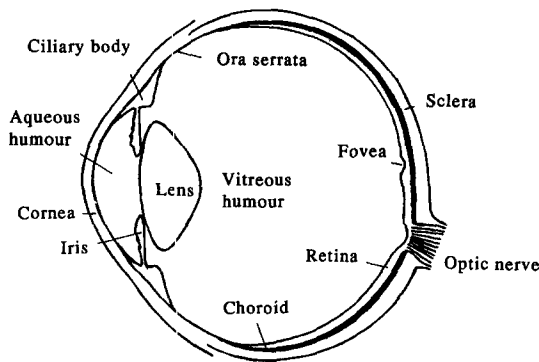


Fig. 1. Section of the human eye.

3. THEORETICAL MODEL

We consider the eye to be formed of seven parts whose thermal properties are distinct: the cornea, the aqueous humour, the lens, the ciliary body, the iris, the vitreous humour and the retina, and suppose that the major modes of heat transfer are the convection of the anterior corneal surface with the surroundings, the internal conduction, the evaporation of the tears film, and the arterial heat transfer from blood flow in the choroid.

Our analytical system is continuous. It is described by a set of partial differential equations. The physical processes are governed by the equation of bioheat transfer in the eye (1):

$$\rho c \frac{\partial T}{\partial t} = \vec{\nabla} \cdot (k \vec{\nabla} T) + H \quad \text{in } \Omega \text{ (inside the eye)} \quad (1)$$

supplemented with boundary condition equations in space (2)–(4)

$$-k \frac{\partial T}{\partial \vec{n}} = h_s (T - T_b) \quad \Gamma_1 \text{ (on sclera)} \quad (2)$$

$$-k \frac{\partial T}{\partial \vec{n}} = h_c (T - T_a) + \sigma \varepsilon (T^4 - T_a^4) \quad \Gamma_2 \text{ (on anterior cornea surface)} \quad (3)$$

$$k \frac{\partial T}{\partial \vec{n}} = 0 \quad \Gamma_3 \text{ (on pupillary axis)} \quad (4)$$

and an initial condition equation (5)

$$T = T(\vec{r}, t = 0) \quad \text{at the time } t = 0 \quad (5)$$

where Ω is the domain studied and $\Gamma_1, \Gamma_2, \Gamma_3$ its boundaries, as indicated in Fig. 2. Values of the thermal conductivity k , the specific heat capacity c and the density ρ required for the seven regions of the eye are assumed constant within each region and with temperature variations. The coefficients h_s and h_c describe the thermal exchanges by convection on the eye surface, respectively, from sclera to body core and from cornea to the surroundings. The radiative exchange is produced on the radiation exposed corneal surface, and the term describing the radiative heat transfer is represented by the Stefan constant σ , and the emissivity ε of the corneal surface, T_a the

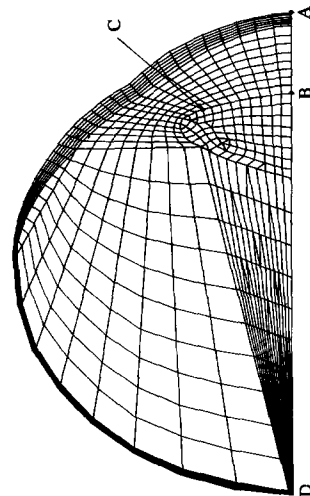


Fig. 2. Two-dimensional meshing of the half section of the eye used in the ocular media-laser interaction study.

ambient temperature, T_b the blood temperature (37°C), \vec{n} the unit vector outward normal, and H the energy density absorbed in the eye tissues. This last term represents the laser heat source.

For an adult human eye, we take the ocular media thermal physical constants values from Scott [5] and Birngruber [4], whereas the thicknesses at the pupillary axis are issued from [8]. These quantities are given in Table 1.

Following Lagendijk [7], we have taken into account the evaporation of the tears film by assuming that $h_c = 14 \text{ W m}^{-2} \text{ }^\circ\text{C}^{-1}$ for the cornea-surrounding heat exchange and $h_s = 65 \text{ W m}^{-2} \text{ }^\circ\text{C}^{-1}$ for convection due to the blood flow in the choroid.

The only initial condition lies in the initial temperature distribution inside the eye. The latter is found by solving equation (1) in the steady state case, neglecting the heat source term, such as:

$$\vec{\nabla} \cdot (k \vec{\nabla} T) = 0 \quad (6)$$

the physical system being subject to the same boundary conditions as stated above, i.e. equations (2)–(4).

3.1. The numerical technique

The mathematical model presented in the previous section is now treated with numerical procedures in order to obtain solutions to the temperature distribution. The system of equations is discretized in two spatial dimensions according to the finite element method and in time according to the widely known finite difference method.

The important steps of the finite element procedure are outlined hereafter. The weighted residue method [9] is applied to the partial differential equations set (1)–(5), and it results in an integral formulation that summarizes the system by the following expression [10]:

Table 1

	k [W m ⁻¹ °C ⁻¹]	ρ [kg m ⁻³]	c [J kg ⁻¹ °C ⁻¹]	Thickness [10 ⁻³ m]
Cornea	0.58	4178	1050	0.6
Aqueous humour	0.58	3997	1000	3.0
Lens	0.40	3000	1050	4.0
Ciliary body	0.58	3997	1000	
Iris	0.58	3997	1000	
Vitreous humour	0.603	4178	1000	15.0
Retina	0.628	4190	1000	0.1

$$W(T) = \int_{\Omega} \langle \psi \rangle \{ L(T) + f_v \} d\Omega = 0 \quad (7)$$

where W is a quantity to minimize, ψ is a weight function, T the admissible solution which satisfies the boundary and initial conditions, L is a derivation operator and f_v the volumic solicitation representing the energy density source term.

In our case, the weight function is taken as equal to δT , and leads to an integral formulation of Galerkin type [9]. We can therefore [10] associate a functional $F(T)$ such that the derivation $(F(T))' = W(T) = 0$. $F(T)$ can be expressed in variational formulation [10] as:

$$F(T) = \langle k \nabla^2 T^2 \rangle - 2\rho c \langle T \delta T / \delta t \rangle + \langle H, T \rangle \quad (8)$$

where the scalar product is defined as:

$$\langle v, u \rangle = \int_{\Omega} v \cdot u d\Omega$$

hence

$$F(T) = k \int_{\Omega} T \nabla^2 T d\Omega - 2\rho c \int_{\Omega} T \frac{\delta T}{\delta t} d\Omega + H \int_{\Omega} T d\Omega \quad (9)$$

Thus, $F(T)$ can be expressed using the Green formula, as the sum of the functions F_1, F_2, F_3 , which are defined below:

$$F_1 = -k \int_{\Omega} (\nabla T)^2 d\Omega - 2\rho c \int_{\Omega} T \frac{\delta T}{\delta t} d\Omega + H \int_{\Omega} T d\Omega$$

(volume term)

$$F_2 = - \int_{\Gamma_1} h_s (T - T_b) d\Gamma_1 \quad (\text{sclera term})$$

$$F_3 = - \int_{\Gamma_2} [Th_c (T - T_a) + \sigma \varepsilon (T^4 - T_a^4)] d\Gamma_2$$

(cornea term).

(10)

A notation describing a quantity X in finite element approximation [10] is introduced as $X = \langle N \rangle \{ X_n \}$ where N represents n interpolation functions and X_n the values of X on the nodes of the elements composing the approximated domain.

After the derivation $\partial F(T) / \partial T$, we obtain for each element the matrix formulation:

$$\left\{ \frac{\partial F}{\partial T} \right\}^e = [k]^e \{ T \}^e + [m]^e \left\{ \frac{\partial T}{\partial t} \right\}^e - \{ g \}^e \quad (11)$$

where

$$[k]^e = -2k \int_{\Omega^e} \langle \nabla N \rangle^T \langle \nabla N \rangle d\Omega^e - (2h_c + \sigma \varepsilon T_F^3) \int_{\Gamma_1^e} \langle N \rangle^T \langle N \rangle d\Gamma_1^e - 2h_s \int_{\Gamma_2^e} \langle N \rangle^T \langle N \rangle d\Gamma_2^e$$

$$[m]^e = -2\rho c \int_{\Omega^e} \langle N \rangle^T \langle N \rangle d\Omega^e$$

$$\{ g \}^e = (h_c T_a + \sigma \varepsilon T_a T_F^3) \int_{\Gamma_1^e} \langle N \rangle^T d\Gamma_1^e + h_s T_b \int_{\Gamma_2^e} \langle N \rangle^T d\Gamma_2^e + H \int_{\Omega^e} \langle N \rangle^T d\Omega^e \quad (12)$$

We have noted $\langle N \rangle^T$ the transposed matrix of $\langle N \rangle$, and make the assumption [12] that $(T^4 - T_a^4) \sim T_F^3 (T - T_a)$, where T_F is the melting temperature of the substance.

Hence we obtain after assembling the elementary matrices, the global system:

$$\frac{\partial F}{\partial T} = \sum_{e=1}^{e=n} \left\{ \frac{\partial F}{\partial T} \right\}^e = [K] \{ T \} + [M] \left\{ \frac{\partial T}{\partial t} \right\} - \{ G \} = 0 \quad (13)$$

where $[K]$ is called the global matrix of stiffness, $[M]$ the global matrix of mass and $\{ G \}$ the global vector of solicitation.

The algebraic system thus obtained is solved by using well known numerical methods (Gauss-Seidel, etc.) to obtain the approximate solution of the temperature distribution.

3.2. The laser deposition

Geometrically, there are three axes in the eye [13], the optical axis, the pupillary axis and the visual axis. For convenience, we choose to mix all three axes in

one. Therefore, the cylindrical symmetry presented suggests the use of the polar coordinates (r, z) .

Taking a half meridional section of the eye globe, the area is subdivided into quadrilateral, triangular and linear elements, see Fig. 2. The elements constitute the different domains representing the eye tissues and the physical thermal constants are thus assigned to the corresponding domain, whereas the peripheral linear elements are involved in the convection heat exchange calculation.

The laser beam falls on the anterior corneal surface, penetrates the transparent ocular media and is absorbed by the different eye tissues along its path. The beam that is focused by the lens is often strongly absorbed in the retina.

The simulation of the laser energy deposition takes into account the irradiance delivered on the anterior surface of the cornea, the aperture of the pupil, the absorption and focalization mechanisms.

The deposited flux on the retina is obtained by the formula taken from [14], that gives its relation with the pupil diameter aperture, the retinal spot diameter and irradiance on the cornea, such as:

$$\frac{E_r}{E_c} = \frac{d_p^2}{d_r^2} \quad \text{with} \quad d_r = 2.44 \frac{\lambda f}{d_p} \quad (14)$$

where λ is the laser wavelength, f the focal distance of the lens ($= 1.7 \times 10^{-2}$ m), d_p the pupil diameter, d_r the laser beam diameter on the retina and E_c the irradiance on the corneal surface.

To deduce the irradiance and the energy density at each node along the laser path, we use the obtained diameter from equation (14) on the retina, the pupil diameter aperture, and the beam diameter at the corneal surface to calculate the intermediate beam diameters in each z position in the eye. Thereafter, the absorbed energy density of each element in laser trajectory is obtained by interpolation.

The energy flux on a node which the coordinates are r and z , on the tissue i is given by:

$$E_i(r, z) = E_0(0, z) \exp(-2r^2/w^2) \exp(-\alpha_i z) \quad (15)$$

where w is the beam-weast and α_i the absorption coefficient of the tissue i , and the energy density absorbed by the tissue i on the node (r, z) is given by:

$$H_i(r, z) = \alpha_i E_i(r, z). \quad (16)$$

Although the model can be applied to any laser wavelength, provided that the absorption parameters of the eye for the wavelength used are available, the main laser wavelengths that have been studied in our simulation are the 1.06×10^{-6} m of the Neodym-YAG laser and the 0.6943×10^{-6} m of the Ruby laser. These wavelengths are widely used in the laboratories and represent electromagnetic radiations in the i.r. and the visible regions. We give in Table 2 the absorption coefficients of the eye tissues for these two lasers. The table shows that the absorption of these laser wave-

Table 2

	Nd-YAG α [m^{-1}]	Ruby α [m^{-1}]
Cornea	113.0	124.0
Aqueous humour	35.0	8.4
Lens	43.5	9.5
Vitreous humour	20.0	2.0
Retina	10000.0	44000.0

lengths is more important on the retina and it is very weak in the other tissues.

In our simulation, the number of elements that absorb the laser radiation is important (about 400 elements). However some results of laser absorption in the ocular media are given in Table 3, where the maximum power density and energy density deposited in each tissue on the pupillary axis are reported, when the laser power is 0.16 W for the Nd-YAG and 0.15 W for the Ruby, the beam diameter on the corneal anterior surface being 8×10^{-3} m for the both lasers, and the pupil aperture diameter is 8.9×10^{-3} m for the Nd-YAG and 7.3×10^{-3} m for the Ruby. With these parameters, the focalization effect of the lens leads to a retinal spot diameter of 4.94×10^{-6} m for Nd-YAG laser and 3.94×10^{-6} m for Ruby laser.

4. RESULTS

In this section we report the results obtained by applying our model using the finite element code MEF/MOSAIC [15] on a SUN Sparc IPC computer. The mesh network is automatically generated after we have determined from the real data the shape of the eye tissues, and differenced them by their physical properties, and also after giving the number of elements wanted in each area.

Thus the finite elements grid used compound 887 elements and 852 nodes. The accuracy of the computed results depends on the density of the grid and the physical parameters used. In the present work, the focal spot being on the retina at the fovea, this region (10^{-4} m toward the choroid) has an intensive grid refinement (116 elements) and a temperature sensitivity study is performed to determine the error range when different physical parameters values given in the literature are used. Hence a steady state calculation is done to obtain the temperature distribution on four reference nodes, Fig. 2, which are the intersection points with the symmetry axis in the case of the nodes (A,B,D) situated on the anterior surfaces of the cornea, the lens, the retina and the node (C) on the germinative zone in other case. The control values of the thermal conductivities that we used in our simulation are taken from Scott [5] and Birngruber [4]. Thus in Table 4, the results obtained with the parameters used in the simulation in one part and the water value of the thermal conductivity in other part, give a maximum temperature difference of 0.8°C ,

Table 3

	Nd-YAG laser		Ruby laser	
	Power density [W m ⁻²]	Energy density [W m ⁻³]	Power density [W m ⁻²]	Energy density [W m ⁻³]
Cornea	0.255 × 10 ⁴	0.288 × 10 ⁶	0.150 × 10 ⁴	0.186 × 10 ⁶
Aqueous humour	0.225 × 10 ⁵	0.787 × 10 ⁶	0.143 × 10 ⁴	0.120 × 10 ⁴
Lens	0.115 × 10 ⁴	0.580 × 10 ⁵	0.137 × 10 ⁴	0.130 × 10 ⁴
Vitreous humour	0.750 × 10 ³	0.150 × 10 ⁵	0.150 × 10 ⁴	0.300 × 10 ³
Retina	0.854 × 10 ⁸	0.854 × 10 ¹²	0.361 × 10 ⁸	0.159 × 10 ¹³

Table 4

	Temperature [°C]			
	A	B	C	D
Water	32.915	33.158	35.047	36.897
Control values	33.713	33.897	35.324	36.861

Table 5

	Temperature [°C]			
	A	B	C	D
Control value	33.713	33.897	35.324	36.861
21 [W m ⁻¹ °C ⁻¹]	33.597	33.778	35.019	36.865
30 [W m ⁻¹ °C ⁻¹]	33.661	33.843	35.264	36.862
54.4 [W m ⁻¹ °C ⁻¹]	33.769	33.954	35.385	36.858

whereas in the region of intensive meshing (D) this difference is 0.03°C.

Otherwise, the temperature sensitivity study for some given literature values of the lens thermal conductivity compared to the control value of the simulation shows, Table 5, a maximum temperature difference of 0.195°C.

The error range on the temperature value is also determined in the following, when the accuracy of the heat transfer coefficients is taken into account. Hence the temperature sensitivity study for the heat transfer coefficient h_c , obtained by comparing some published values to the Legendijk's coefficients that we used in our simulation gives, Table 6, a maximum temperature difference of 0.643°C for h_c values that vary between 10 and 15 W m⁻² °C⁻¹.

Table 6

	Temperature [°C]			
	A	B	C	D
Control value	33.713	33.897	35.324	36.861
10 [W m ⁻² °C ⁻¹]	34.234	34.391	35.595	36.883
12 [W m ⁻² °C ⁻¹]	33.968	34.138	35.456	36.872
15 [W m ⁻² °C ⁻¹]	33.591	33.781	35.259	36.855

Whereas this difference, Table 7, is 0.167°C for h_c values between 65 and 11 W m⁻² °C⁻¹.

We can thus conclude that the maximum temperature variation due to the accuracy of the parameters used is less than 1°C for the thermal conductivities and less than 0.65°C for the heat transfer coefficients. These values may constitute the error range of the approximated temperature distribution obtained.

Taking into account these considerations, we begin the simulation of laser induced heat transfer in the human eye by obtaining the temperature distribution in the steady-state case without the heat source term, when the eye is only submitted to the convection that is due to heat exchanges between the corneal surface and the surrounding and that due to the blood flowing in the choroid. Moreover a strong nonlinearity due to the radiation term is present. Thus, Fig. 3 gives the temperature distribution on the pupillary axis, and as it can be seen, the temperature varies between 33.7°C on the cornea and 36.9°C on the sclera. In addition the isotherm curves obtained for the total domain are reported in Fig. 4. We can deduce from the results obtained in the nonlinear steady state resolution that we are in good agreement with those of refs. [5-7] and thus the temperature distribution issued for the entire domain is that which is used as the initial conditions for the transient and permanent regime simulation study.

The solution of the non-steady-state problem is obtained by including the heat source term that represents the laser energy density in the heat equation associated to the boundary conditions represented by the convection heat transfers and the initial conditions given by the steady state temperature distribution obtained above. The laser beam path inside the eye is simulated by the appropriate grid, Fig. 2, and each laser affected element absorbs a quantity of energy.

Table 7

	Temperature [°C]			
	A	B	C	D
Control value	33.713	33.897	35.324	36.861
90 [W m ⁻² °C ⁻¹]	33.825	34.012	35.453	36.916
110 [W m ⁻² °C ⁻¹]	33.858	34.045	35.491	36.929

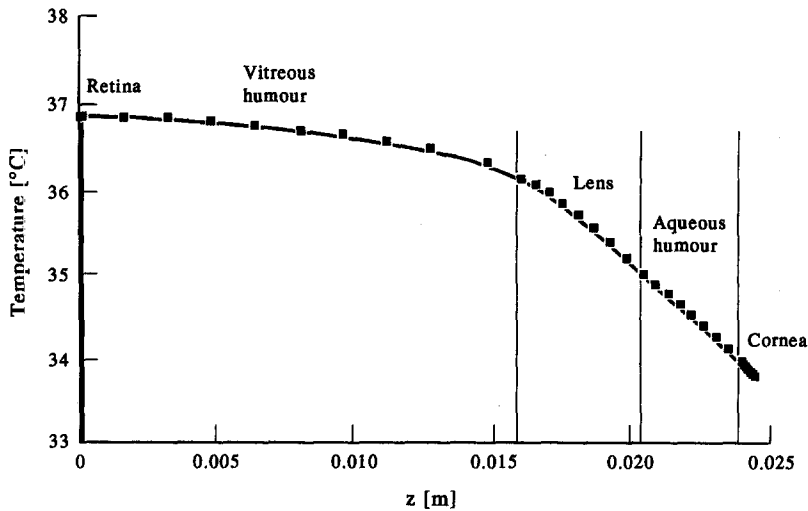


Fig. 3. Spatial distribution of the temperature on the pupillary axis in the steady-state case without heat source.

On Fig. 5, we can see the results given by the model for a 0.15 s laser exposition at 0.16 W laser power, 8×10^{-3} m laser beam diameter on corneal surface, and for different pupil diameter apertures. The Nd-YAG laser effects are compared to a 0.15 s Ruby laser exposition for the same laser parameters with 7×10^{-3} m pupil diameter aperture. One can deduce that the lowest wavelength is the most absorbed by the retinal surface, and that the deposited energy density for the Nd-YAG increases with the pupil diameter aperture. The maximum retinal temperature during laser exposition is reached after few milliseconds and the laser switching off leads to a fast drop in temperature. Birngruber *et al.* [4] has used as a domain, in the

analytical model on retinal injury, the different layers of the retinal tissue and the results obtained with the Nd-YAG laser case give a maximum temperature of 74°C for 0.15 s exposition, 0.16 W laser power, and a retinal diameter spot of 13×10^{-6} m. Our model that takes into account the trajectory of the laser beam inside the eye, its focalization and absorption, and pupil aperture, gives the corresponding curve to Birngruber's result when the beam diameter on corneal surface is 8×10^{-3} m, the lens focal is 17×10^{-3} m, the beam power is 0.16 W and the pupil diameter aperture is 9×10^{-3} m.

And to compare the Birngruber *et al.* results for Ruby laser study, we present in Fig. 6 the temperature profile given by the simulation for a 10^{-3} s Ruby exposition, and the relaxation when the laser source is cancelled. The parameters used are 0.15 W laser power, 8×10^{-3} m beam diameter on corneal surface and 7×10^{-3} m pupil diameter aperture. Birngruber *et al.* have used in the analytical model 0.15 W beam power, 1 ms exposition and 16×10^{-6} m beam spot on the retina and have obtained a maximum temperature of 97°C .

As it is noticed above, the eye and the laser characteristics play an important role. To make evident the influence of some parameters, such as the beam power, the pupil aperture and the beam diameter on the corneal surface, we give in Fig. 7 the evolution of the temperature vs the laser power for a medium pupil diameter aperture. It appears that for the Nd-YAG laser the increase of the temperature with the laser power is weak compared to that with the Ruby laser and this is due to the concentration of the energy on the retinal spot which is higher in the case of the Ruby laser. In Fig. 8 the dependence of the retinal temperature with pupil diameter aperture makes evident the importance of this parameter, as the iris becomes larger the maximum retinal temperature

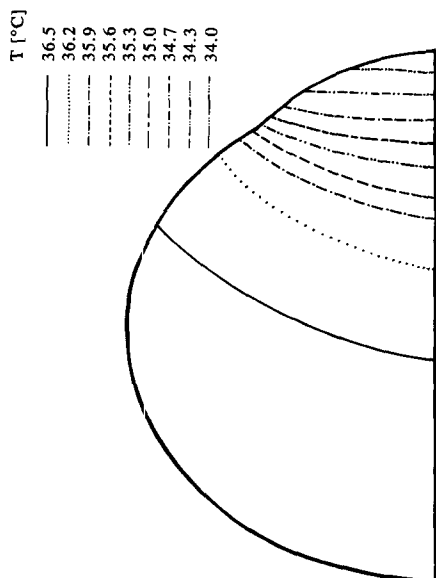


Fig. 4. Isotherm curves inside the eye in the steady-state case without heat source.

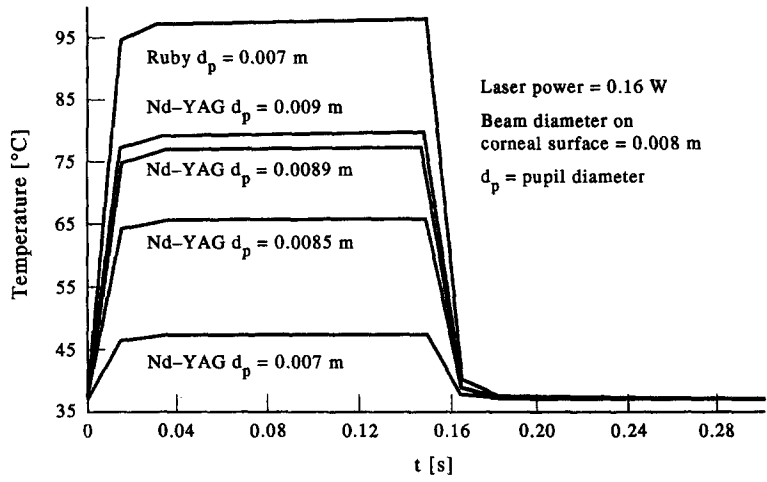


Fig. 5. Maximum retinal temperature evolution for a 150 ms laser exposition. Different pupil diameter are checked in case of Neodym-YAG laser.

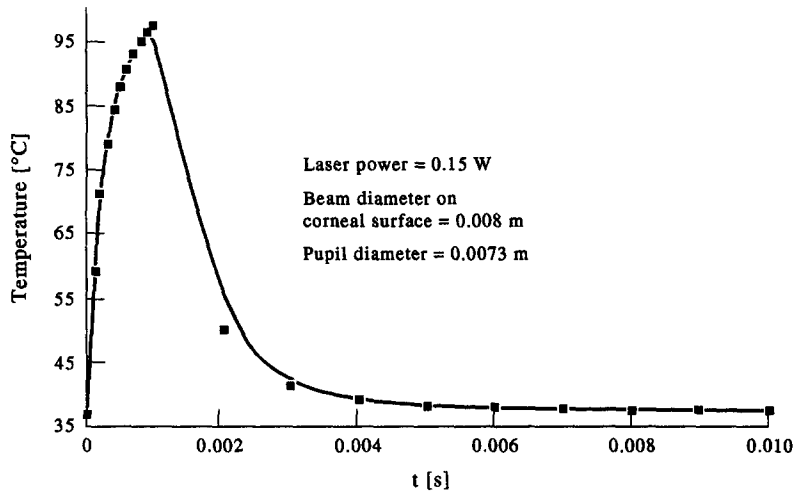


Fig. 6. Maximum retinal temperature evolution for a 1 ms Ruby exposure and relaxation after source cancelling.

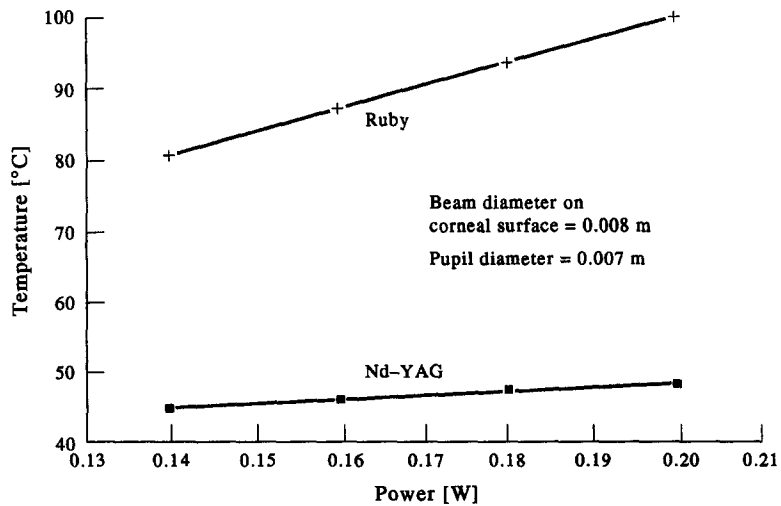


Fig. 7. Maximum retinal temperature dependence on the laser power for a 1 ms exposure.

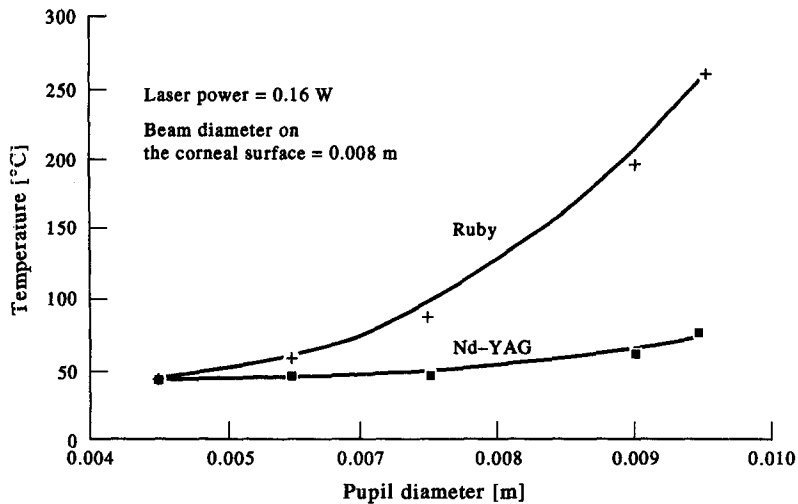


Fig. 8. Maximum retinal temperature dependence on the eye pupil diameter aperture for a 1ms laser exposure.

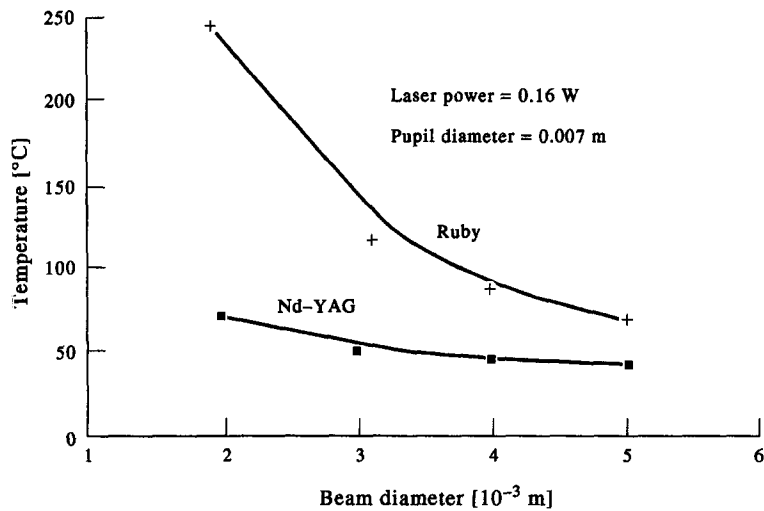


Fig. 9. Maximum retinal temperature dependence on the laser beam diameter at the anterior corneal surface for a 1ms laser exposure.

obtained for the Ruby laser is more important. It is obvious that beyond 100°C the tissue is destroyed and hence the evolution presented for the Ruby laser when the pupil diameter is great than 7.5×10^{-3} m is not realistic. The influence of the beam diameter on the corneal surface on maximum retinal temperature is shown in Fig. 9. It appears that as the beam diameter decreases, the temperature increases, and this is due to the value of the irradiance on the cornea which has an inverse dependance with the square diameter of the laser spot. We conclude this results section by giving a sample of a temperature distribution in the eye when

the laser source is present. Figure 10 shows the global isothermperature curves with the enlarging of the retinal spot region.

5. CONCLUSION

In this contribution, we studied the evolution of the temperature as function of laser irradiance parameters and eye characteristics. The results obtained by using our model for laser-human eye interaction seem to be realistic and are close to those obtained by other authors. However, everybody has complained about

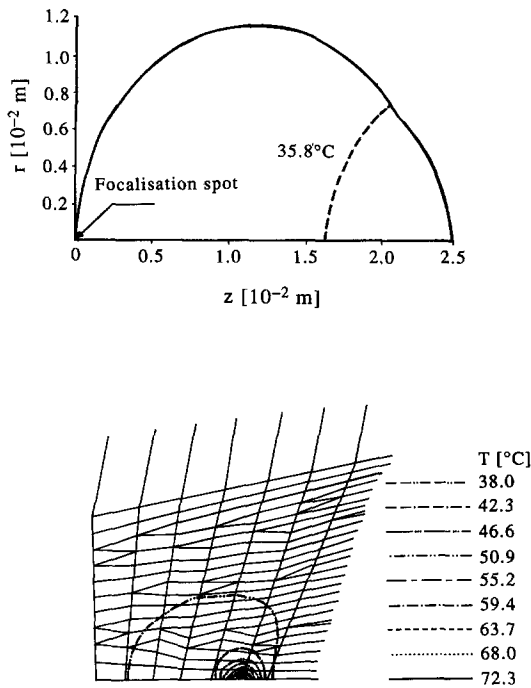


Fig. 10. Isotherm curves distribution for the entire eye with the enlarging of the the focalization spot region.

the lack of informations on the real values of the physical parameters of the human eye tissues, due to the necessity of *in-vivo* experiments. The model can be enhanced by coupling the thermal aspect discussed here to the fluid problem of the blood flow in the eye tissues.

Acknowledgements—The author is grateful to Professors Reginald Birngruber and Peter J. Wainwright, for providing some papers dealing with the subject treated in this study and tables of physical characteristics of the ocular media.

REFERENCES

1. D. H. Sliney, *Proceedings of the First Symposium on the Biological effects Hazards and Protection from Non-Ionizing Radiation in Outdoor Applications*, 12–17 August 1987, Stockholm, Special Issue, *Health Phys.* **56**(5) (May 1989).
2. P. Kramar, C. Harris, A. F. Emery and A. W. Guy, Acute microwave irradiation and cataract formation in rabbits and monkeys, *J. Microwave Power* **13**(3), 239–288 (1978).
3. A. F. Emery, P. Kramar, A. W. Guy and J. C. Lin, Microwave induced temperature rises in rabbit eyes in cataract research, *Trans. ASME, J. Heat Transfer* **C97**, 123–131 (1975).
4. R. Birngruber, F. Hillenkamp and V. P. Gabel, Theoretical investigations of laser thermal retinal injury, *Health Phys.* **48**(6), 781–797 (1985).
5. J. A. Scott, A finite element model of heat transport in the human eye, *Phys. Med. Biol.* **33**(2), 227–242 (1988).
6. J. A. Scott, The computation of temperature rises in the human eye induced by infrared radiation, *Phys. Med. Biol.* **33**(2), 243–257 (1988).
7. J. J. W. Lagendijk, A mathematical model to calculate temperature distributions in human and rabbit eyes during hyperthermic treatment, *Phys. Med. Biol.* **27**(11), 1301–1311 (1982).
8. Y. Le Grand and S. G. El Hage, *Physiological Optics*, pp. 25–55. Springer Series in Optical Sciences, Springer, New York (1980).
9. O. C. Zienkiewicz, *The Finite Element Method in Engineering Science* (3rd Edn). McGraw-Hill, New York (1977).
10. G. Dhatt and G. Touzot, *Une Presentation de la Methode des Elements Finis*. Les Presses de l'Universite Laval Quebec, Paris (1981).
11. D. Kechemair, Contribution à l'étude de l'interaction laser–matière, Thèse de Doctorat en Science, p. 69, Université de Paris XI (1989).
12. D. Kechemair, Contribution à l'étude de l'interaction laser–matière, Thèse de Doctorat en Science, p. 64, Université de Paris XI (1989).
13. Y. Le Grand and S. G. El Hage, *Physiological Optics*, p. 73. Springer Series in Optical Sciences, Springer, New York (1980).
14. H. Cember, *Introduction to Health Physics* (2nd Edn), p. 422. Pergamon Press, Oxford (1987).
15. Framasoft and Compiègne Science Industrie, MEF /MOSAIC, Reference Manual, France (1991).